

ORIGINAL RESEARCH REPORT

Combination of biocompatible hydrogel precursors to apatitic calcium phosphate cements (CPCs): Influence of the in situ hydrogel reticulation on the CPC properties

Silvia Stella Ramirez Caballero¹ | Daniel Ferri-Angulo² | Romain Debret³ | Fabien Granier⁴ | Sébastien Marie⁴ | François-Xavier Lefèvre⁵ | Jean-Michel Bouler⁵ | Christelle Despas⁶ | Jérôme Sohier² | Bruno Bujoli⁵ 

¹Graftys Discovery SA, UFR Sciences et Techniques, Nantes, France

²Université Lyon, INSA Lyon, UMR 5510 CNRS, MATEIS, Villeurbanne, France

³UMR 5305 CNRS, Laboratory of Biology Tissue and Therapeutic Engineering LBTI, Lyon, France

⁴Colcom, Cap Alpha, Clapiers, France

⁵Université de Nantes, CNRS, UMR 6230, CEISAM, UFR Sciences et Techniques, France

⁶Nancy-Université, CNRS, UMR 7564, LCPME, Villers-lès- Nancy, France

Correspondence

Bruno Bujoli, Université de Nantes, CNRS, UMR 6230, CEISAM, UFR Sciences et Techniques2, rue de la Houssinière, BP 92208, 44322 Nantes Cedex 3, France.
Email: bruno.bujoli@univ-nantes.fr

Funding information

BPI-France (23rd call for R&D proposals of FUI), Grant/Award Number: DOS0056563/00; Graftys; COLCOM

Abstract

In the field of bone regenerative medicine, injectable calcium phosphate cements (CPCs) are used for decades in clinics, as bone void fillers. Most often preformed polymers (e.g., hyaluronic acid, collagen, chitosan, cellulose ethers...) are introduced in the CPC formulation to make it injectable and improve its cohesion. Once the cement has hardened, the polymer is simply trapped in the CPC structure and no organic subnetwork is present. By contrast, in this work a CPC was combined with organic monomers that reticulated in situ so that a continuous biocompatible 3D polymeric subnetwork was formed in the CPC microstructure, resulting in a higher permeability of the CPC, which might allow to accelerate its in vivo degradation. Two options were investigated depending on whether the polymer was formed before the apatitic inorganic network or concomitantly. In the former case, conditions were found to reach a suitable rheology for easy injection of the composite. In addition, the in situ formed polymer was shown to strongly affect the size, density, and arrangement of the apatite crystals formed during the setting reaction, thereby offering an original route to modulate the microstructure and porosity of apatitic cements.

KEYWORDS

apatitic cement, composite biomaterial, microstructure, reticulated hydrogel

1 | INTRODUCTION

The use of calcium phosphate cements (CPCs) (Brown & Chow, 1983; LeGeros, Chohayeb, & Shulman, 1982; Mirtchi, Lemaitre, & Terao, 1989) as bone substitutes in clinics is rapidly expanding, in particular in trauma surgery (Bajammal et al., 2008; Carey, Xu, Simon, Takagi, & Chow, 2005; Larsson & Bauer, 2002; Larsson & Hannink, 2011). Similar to calcium phosphate bioceramics, CPCs show excellent biocompatibility, bioactivity, and osteoconductivity, leading to their replacement by bone over a few months, thanks to the natural bone remodeling process. When injectable, they offer the possibility for filling bone voids of any shape, under minimally invasive conditions

(Bohner, Gbureck, & Barralet, 2005; Dorozhkin, 2008; Dorozhkin, 2013; Ginebra, Espanol, Montufar, Perez, & Mestres, 2010; Khairoun et al., 2002). In this context, the latest improvements to confer suitable injectability (Bohner & Baroud, 2005; Habib, Baroud, Gitzhofer, & Bohner, 2008; Khairoun, Boltong, Driessens, & Planell, 1998; O'Neill et al., 2017) and cohesion (Bohner, Doebelin, & Baroud, 2006; Chen, Li, Yu, & Sun, 2009) to CPCs, and tune their mechanical properties (Fernandez et al., 1998; Johnson & Herschler, 2011; Zhang, Liu, Schnitzler, Tancret, & Bouler, 2014; Zhang, Tancret, & Bouler, 2011) and porosity (del Real, Ooms, Wolke, Vallet-Regi, & Jansen, 2003; Gauthier, Bouler, Aguado, Pilet, & Daculsi, 1998; Xu, Takagi, Quinn, & Chow, 2004), most often include the introduction of polymer

additives in the CPC formulation (e.g., sodium alginate, hyaluronic acid, collagen, polypeptides, chitosan, cellulose ethers...) (Alkhraisat et al., 2009; Burguera, Xu, & Weir, 2006; Cherng, Takagi, & Chow, 1997; Ishikawa, Miyamoto, Kon, Nagayama, & Asaoka, 1995; Jyoti, Thai, Min, Lee, & Song, 2010; Khairoun, Driessens, Boltong, Planell, & Wenz, 1999; Lin et al., 2006; Liu et al., 2006; Liu et al., 2014; Liu, Zhang, Weiss, Tancret, & Bouler, 2013; Miyamoto et al., 1998; Song, Rahman, & Lee, 2009; Tajima, Nishimoto, Kishi, Matsuya, & Ishikawa, 2004; Takagi, Chow, Hirayama, & Eichmiller, 2003; Thai & Lee, 2010; Wang, Chen, Xiang, & Ye, 2007; Xu & Simon, 2005; Zhang et al., 2016) Interestingly, these polymers solubilized in the intergranular space of the cement paste often contribute to avoid phase separation between the liquid and solid components of the CPC and provide suitable rheology for an easy injection through a syringe needle.

In the early stage of the setting reaction of apatitic CPCs, precipitation of apatite crystals occurs quite rapidly in the intergranular space initially occupied by the liquid phase (containing additives or not). The entanglement of these crystals then leads to a hardened material. Depending on the nature of the CPC, this reaction starts a few minutes (~2–5 min) after mixing the CPC liquid and solid phases and usually ends up after a 10–40 min period (Despas et al., 2014). When a preformed polymer (e.g., hyaluronic acid, collagen, chitosan, cellulose ethers...) is present in the CPC formulation, the latter is simply trapped in the CPC structure once the cement has hardened and does not influence that much the cement microstructure since no organic sub-network is present. In this context, we were interested to investigate whether the introduction of organic monomers that would self-assemble in situ concomitantly or even before the CPC setting process might influence the microstructure of the hardened CPC. Indeed, the formation of a continuous biocompatible 3D polymeric sub-network might result in a higher permeability of the CPC, which might allow to accelerate its *in vivo* degradation. With these considerations in mind, the precursor candidates selected for this study were based on poly(L-lysine) dendrigrafts (DGL) and polyethylene glycol homobifunctionalized with N-hydroxysuccinimide (PEG-NHS). PEG is indeed a bio-inert polymer approved by the FDA for several medical applications (Drury & Mooney, 2003) while DGL are non-immunogenic dendrimers of low cytotoxicity (Francoia & Vial, 2018; Romestand et al., 2010). When these two products are mixed in aqueous solution, the reticulation process is driven by the reaction of the activated ester end-groups of PEG-NHS with the alpha and epsilon amine groups of DGL which creates a 3D network through the formation of stable amide bonds in physiologic to slightly alkaline conditions (pH 7.2–9) (Debret, Faye, Sohier, & Sommer, 2017). N-hydroxysuccinimide (NHS) is concomitantly released as a result of this condensation reaction (Figure 1). More importantly, depending on the concentration of the two hydrogel precursors, the crosslinking time in phosphate-buffered saline can be varied between a few seconds to a few minutes, as well as the mechanical properties of the hydrogels, with a complex modulus ranging from a few to 100 kPa. Furthermore, this hydrogel was shown to be noncytotoxic and to act as a support promoting cellular attachment and proliferation, while being

biocompatible and degraded *in vivo* through phagocytosis by macrophages (Debret et al., 2017; Lorion et al., 2014). As such, it was shown to have great potential to stimulate skin wound healing, thus making very attractive its assessment in the context of bone regeneration and repair.

2 | MATERIALS AND METHODS

2.1 | Chemicals

Two apatitic CPCs were used in this study:

- Graftys[®] HBS [abbreviated as HBS], obtained from Graftys SA (Aix-en-Provence, France), is a mixture of 78 wt.% α -tricalcium phosphate (α -TCP) ($\text{Ca}_3(\text{PO}_4)_2$), 5 wt.% dicalcium phosphate dihydrate (DCPD) ($\text{CaHPO}_4 \cdot 2\text{H}_2\text{O}$), 5 wt.% monocalcium phosphate monohydrate ($\text{Ca}(\text{H}_2\text{PO}_4)_2 \cdot \text{H}_2\text{O}$), 10 wt.% calcium-deficient hydroxyapatite (CDA) ($\text{Ca}_{10-x}[\]_x(\text{HPO}_4)_y(\text{PO}_4)_{6-y}(\text{OH})_{2-z}[\]_z$), and 2 wt.% hydroxypropyl methyl cellulose (HPMC). The liquid phase consisted of a 2 or 5 wt.% Na_2HPO_4 aqueous solution (liquid/powder ratio = 0.5 ml g^{-1}).
- An HPMC-free analog of Graftys HBS [abbreviated as HBS-0] was specially prepared for this study, under the same conditions except that no HPMC was added to the fabrication process.

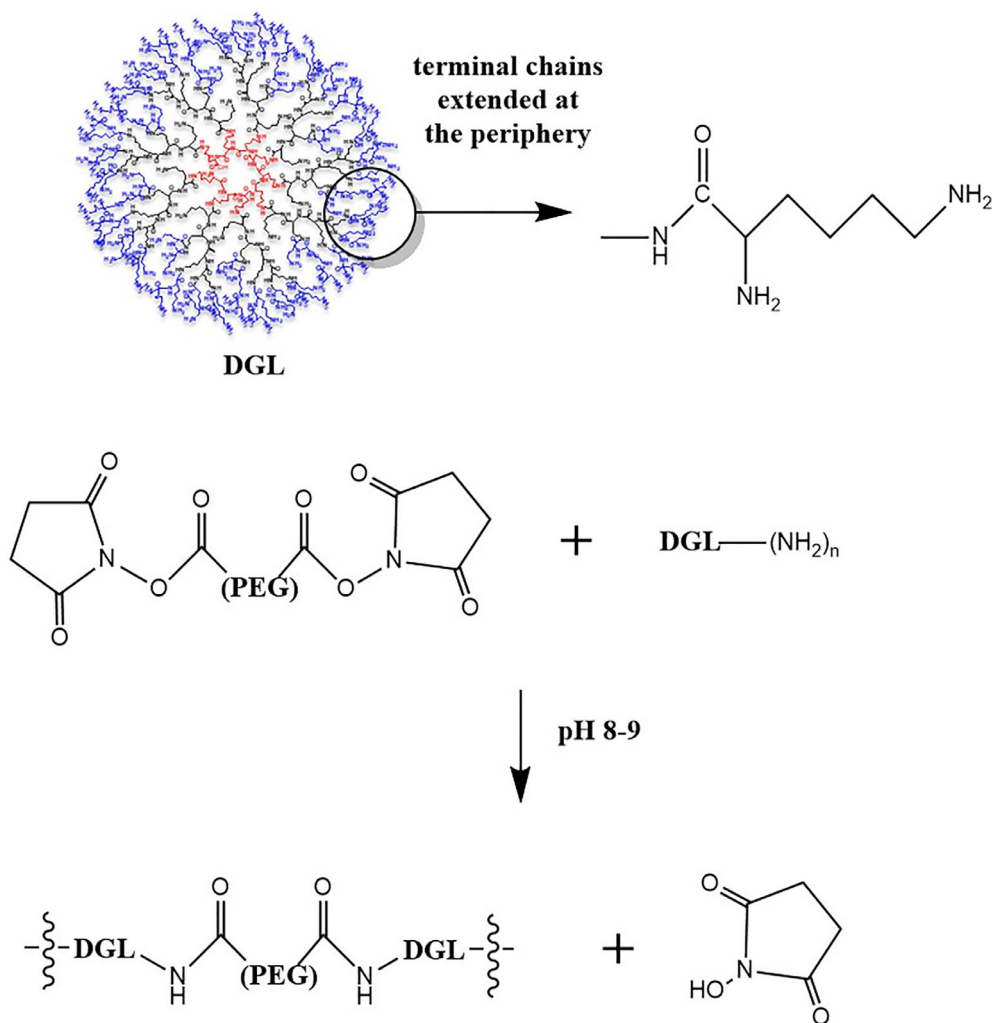
A 10 kDa polyethylene glycol chain end-capped with two N-hydroxysuccinimide groups (noted PEG-NHS) was obtained from Sigma-Aldrich (ref 713797, CAS 186020-53-1). A third-generation poly(L-lysine) dendrigraft (noted DGL) was obtained from COLCOM and prepared as previously reported (Collet et al., 2010). TFA-L-Lys-NCA being used as monomers for the polymerization process, the synthesis leads to poly-cationic polymers of L-Lysine with protonated amino groups associated with trifluoroacetate (noted TFA) counter ions after deprotection of the ϵ -amines of the Lysine units. The last step consisted of an exchange of the TFA counter ions by chloride, via the addition of a large excess of a sodium chloride aqueous solution. Then the free salts were removed by ultrafiltration using a 5-kDa cut off. Residual TFA was lower than 1% as controlled by ^{19}F NMR.

2.2 | Preparation of the CPC formulations

HBS and HBS-0 cement samples were prepared by mixing 5 g of the powdered preparation with their liquid phase for 1 min to ensure the homogeneity of the resulting paste before use.

For the preparation of the composite, a DGL/PEG-NHS weight ratio of ~0.16 was selected for this study (Debret et al., 2017). The required amount of solid PEG-NHS was first dispersed in 5 g of the HBS-0 CPC powder, and the two products were mixed in a mortar, using a pestle. On the other hand, the required amount of DGL powder was dissolved in 2.5 ml of a Na_2HPO_4 aqueous solution (either 2 or 5 wt.%). In a final step, the DGL solution was added to the CPC/

FIGURE 1 Schematic structure of poly(L-lysine) dendrigraft (DGL); a schematic representation of the reticulation process resulting from the reaction of polyethylene glycol homobifunctionalized with N-hydroxysuccinimide (PEG-NHS) and DGL



PEG-NHS powder, and the resulting mixture was mixed in a mortar for 1 min to obtain a homogeneous paste. The resulting composite was then noted 8/50, 16/100, 24/150, or 40/250, where for example 24/150 corresponds to a DGL concentration of 24 mg ml⁻¹ and a PEG-NHS concentration of 150 mg ml⁻¹, with respect to the liquid phase (i.e., the Na₂HPO₄ aqueous solution).

To investigate the properties of the different cements prepared in this study (mechanical properties and microstructure), specimens of cylindrical shape (6 mm in diameter and 12 mm of length) were prepared by pressing the resulting pastes into Teflon molds using a spatula. The molds containing the paste were immersed in a saline solution (0.9 wt.% sodium chloride aqueous solution), then incubated in a homothermal oven at 37°C for 72 hr or 1 week, before being polished to obtain flat and parallel faces for the bulk specimens, which were then unmolded.

To investigate whether a 3D-organic network had formed in the different hydrogel-containing cement composites once hardened, decalcification of the samples was performed by immersion of cylindrical cement blocks (diameter: 8 mm, height: 5 mm, and hardening time: 1 week) in 30 ml of a 10 wt.% aqueous solution of ethylenediaminetetraacetic acid (EDTA) at room temperature for

2 weeks, with a renewal of the EDTA solution every ~5 days. At the end of this treatment, the samples were immersed successively in water (10 ml, 2 days), 95% ethanol (30 ml, 3 days), and pure ethanol. The samples were then rinsed in water/acetone mixtures of increasing content in acetone, to end-up with rinsing with pure acetone. Finally, the samples were dried by applying 12 cycles of rinsing with supercritical carbon dioxide. Similar experiments run with conventional HBS or HBS-0 led to full dissolution of the corresponding cement blocks, by contrast with the hydrogel-containing composites that in most cases retained their initial shape.

2.3 | Methods

2.3.1 | SEM experiments

The measurements were carried out on cylindrical cement blocks allowed to harden for 1 week (see Section 2.2). Then, a 1 mm² polished cross-section of the samples was obtained using a JEOL cross-section polisher SM09010, by applying an argon ion beam accelerated by a voltage from 4.5 to 6 kV perpendicular to the surface

of each specimen for 4–8 hr. SEM observation of those samples was performed using a Field Emission Gun Scanning Electron Microscope (Jeol 7600F). Images were acquired on a backscattered electron mode with an 8 pA beam current and an 8 kV accelerated voltage.

2.3.2 | Compressive strength measurements

The measurements were carried out on cylinder-shaped molded samples under wet conditions (hardening time: 72 hr), that is, immediately after taking the specimens out of the hardening solution (see Section 2.2). A TAHD+ texture analyzer was used and the samples were submitted to increasing compression load (displacement of the compressive rig: 1 mm s^{-1}), the profile of which was recorded until fracture.

2.3.3 | Dynamic mechanical analyses

The dynamic properties of the CPC references, hydrogels, and CPC composites were determined using a Dynamic Mechanical Analyser (NETZCH DMA 242E Artemis and DMA 242E, TASC414/4 and CS200LT as controllers) at room temperature. The variation of the mechanical phase angle tangent ($\tan \delta$) versus time was thus recorded, this parameter corresponding to the ratio between the dynamic loss modulus (E'') and dynamic storage modulus (E') ($\tan \delta = E''/E'$). The evolution of $\tan \delta$ is representative of changes in the viscosity of the samples, the higher the $\tan \delta$ value, the greater the viscosity of the materials, and the onset point of the $\tan \delta$ versus time curve (Proteus[®] software) was thus used to assess the time at which the phase transitions occurred.

In a typical experiment, DGL was dissolved in a 2 or 5 wt.% Na_2HPO_4 aqueous solution (200 μl , at different concentrations: 8, 16, 24, or 40 mg ml^{-1} , respectively). Afterward, this solution was added to the desired crushed solid placed in a $12 \times 6 \text{ mm}$ cupula, that is, either pure PEG-NHS or PEG-NHS mixed with 400 mg of HBS-0, so that the final concentration of PEG-NHS with respect to the liquid phase was 50, 100, 150, or 250 mg ml^{-1} , with a DGL/PEG-NHS ratio of 0.16. The resulting mixture was mixed by hand for approximately 1 min at room temperature in the cupula. An $8 \times 4 \text{ mm}$ rod connected to the DMA and undergoing a sinusoidal vertical movement of 100 μm at 10 Hertz was then immediately immersed in the sample, allowing to record the $\tan \delta$ value versus time. Additionally, the cement HBS-0 reference (with no DGL or PEG-NHS) was also studied for comparison.

2.3.4 | High-frequency impedance measurements

The high-frequency impedance measurements were recorded, between 0.4 and 100 MHz, with an HP 4194 A impedance/gain-phase analyzer (Hewlett-Packard) at 37°C , using an experimental setup reported previously (Despas et al., 2014).

The experimental device was completed by a computer allowing automatic data acquisition and real-time calculation of the complex impedance, Z^* from which the dielectric permittivity, ϵ' (related to dipole variation), and dielectric losses, ϵ'' (related to the motion of free charges) were computed. (Thiebaut, Roussy, Chlihi, & Bessiere, 1989)

2.3.5 | Injectability and cohesion assessment

An AMETEK LS5 texture analyzer was used to assess the injectability of the different samples 15 min after starting the paste preparation. This consisted of measuring the compression force necessary to extrude the cement paste samples from a syringe (inner diameter of the cartridge 8.2 mm, inner diameter of the exit hole 1.7 mm, extrusion rate 1 mm s^{-1} at 15 min). In the end, the percentage of paste extruded was determined.

Cohesion assessment was conducted 5 and 15 min after starting the paste preparation. For that purpose, the paste was directly extruded into a 0.9 wt% NaCl solution, and a visual check of the extruded filaments was done 24 hr after extrusion, showing either shape retention or disaggregation depending whether the paste was cohesive or not.

2.3.6 | Statistical analysis

For DMA, each measure of $\tan \delta$ was repeated three times per condition. For the obtained experimental results, statistical analyses were performed with Statgraphics (Statgraphics Technologies, VA). Data values are presented as mean \pm SE and conditions were compared with a multiple-sample comparison test with a least significant difference post hoc analysis, for a 95% confidence level ($p < .05$).

For each condition, the high-frequency impedance experiments were duplicated and the SD on deduced initial and final setting times was estimated to be between 1 and 6%, consistent with previous similar studies performed on other CPC systems (Despas et al., 2014).

For the injectability assessment, analysis of variance (ANOVA) was performed on the applied extrusion force data for the HBS-0 and CPC composites samples prepared using 2 or 5 wt.% aqueous Na_2HPO_4 , with $\alpha = .05$ (meaning that, for $p < .05$, at least one group of samples was statistically different compared with the other groups). To identify the sample or samples that was/were significantly different, a statistical study for each applied extrusion force result was carried out using F-test followed by a two-tailed t-test (two-tail analysis).

For the compressive strength measurements, six cylinders were used for each sample to calculate the mean and SD. ANOVA was performed on the compressive strength data for the HBS-0 and CPC composites samples prepared using 2 or 5 wt.% aqueous Na_2HPO_4 , with $\alpha = .05$ (meaning that, for $p < .05$, at least one group of samples was statistically different compared with the other groups). To identify the sample or samples that was/were significantly different, a statistical study for each mechanical result was carried out using F-test followed by a two-tailed t-test.

3 | RESULTS

To make sure that the hydrogel formation only starts once the cement paste is prepared, one of the two hydrogel precursors was combined to the solid phase of the CPC while the other was dissolved in the liquid phase. To minimize the undesired hydrolysis of the N-hydroxysuccinimide groups, the PEG-NHS compound was mixed with the cement powder.

3.1 | Behavior of the hydrogel precursors under the conditions of the CPC workup

In a first step, the solubility of the PEG-NHS and DGL compounds in the CPC liquid phase (i.e., 5 wt.% Na_2HPO_4) was investigated, showing that DGL is soluble in this medium (up to 40 mg ml^{-1}). On the other hand, the solubility limit of PEG-NHS was only 180 mg ml^{-1} but was found to be shifted to 910 mg ml^{-1} in a 2 wt.% Na_2HPO_4 solution. Then the formation of the hydrogel was assessed in a 5 wt.% Na_2HPO_4 solution, respectively, below (DGL: 24 mg ml^{-1} , PEG-NHS: 150 mg ml^{-1} , noted 24/150) and above (40/250) the PEG-NHS solubility limit. After a 30 min crosslinking time, the resulting hydrogel was rinsed three times with water and dried. When operating below the PEG-NHS solubility limit (e.g., 24/150) the amount of recovered solid was $\sim 90\%$ of the initial mass of reagents, while it dropped to 66% when operating above the PEG-NHS solubility limit (e.g., 40/250), giving evidence that part of the PEG-NHS was unreacted in that case and then washed out of the hydrogel during the rinsing steps.

3.2 | Monitoring of the setting time of the CPC composites by high-frequency impedance measurements

During the hardening process of apatitic CPCs, the major component of the solid phase (alpha-tricalcium phosphate, noted α -TCP) slowly dissolves, leading to a saturation of the liquid phase in calcium and phosphate ions, which results in the rapid precipitation of less soluble and thermodynamically more stable calcium phosphate in the intergranular space, that is, CDA. The entanglement of these apatite crystals makes the CPC harden. High-frequency impedance was used to monitor this reaction (Despas et al., 2014) and the recorded complex impedance data allowed to deduce the profile of:

(a) the dielectric permittivity (ϵ') that showed a rapid increase due to the accumulation of mobile unbound charged species on the surface of the solid reactants leading to a supersaturated solution, followed by a maximum corresponding to a full coverage of the α -TCP surface by a semipermeable CDA shell; then an aging period takes place, characterized by a constrained diffusion of water and ions toward the inner part of the α -TCP particles and the formation of a less conductive final setting product;

(b) dielectric losses (ϵ''), which are related to the motion of free charges, which decrease as the precipitation of apatite starts leading to a progressive hardening of the cement paste.

In a final step, when the diffusion of reactive species through the CDA layer gets too limited, dielectric parameters reach a constant value. Therefore, the evolution of the ϵ' and ϵ'' experimental values during the setting reaction was recorded for the different composites, by comparison with the corresponding polymer-free references (Table 1; Figure 2 and Figure S1).

Under standard conditions (no hydrogel precursor—5 wt.% Na_2HPO_4), the hydrolysis of α -TCP, promoted by Na_2HPO_4 , started rapidly after mixing the liquid and solid components resulting in precipitation of CDA in the intergranular space over a ~ 40 min period. This was evidenced by the variation of the dielectric parameters which was quite smooth during the first 20 min, before getting sharper (ϵ' (large \uparrow) and ϵ'' (rapid \downarrow)). When the hydrogel precursors were added in the cement composition, the same trend was observed although the CDA precipitation in the intergranular space extended for a longer period in direct proportion with the amount of hydrogel precursors loaded in the cement composition (i.e., ~ 40 min for 16/100; ~ 70 min for 24/150—Figure S1).

By contrast, when the phosphate concentration in the liquid phase was lower (i.e., 2 wt.% Na_2HPO_4), the precipitation of apatite in the intergranular space was significantly delayed in the absence of any additive, as shown by the ϵ' value which remained almost constant for 1 hr before the CDA precipitation started (0/0—Figure 2). Interestingly, when increasing amounts of hydrogel precursors were combined to the CPC, the initiation of the setting reaction was more and more shifted toward longer times (from 160 min for 16/100 to 375 min for 40/250) and the CDA precipitation occurred over a longer period (~ 170 min versus 40 min for the undoped HBS-0 reference).

3.3 | Dynamic mechanical analyses

Dynamic mechanical analysis (DMA) was used to monitor changes in the energy dissipation of the CPC references, hydrogels, and CPC composites, under cyclic loading as a function of time.

In a first experiment, a solution of DGL in aqueous Na_2HPO_4 (2 or 5 wt.%) was mixed for 1 min with the solid form of PEG-NHS, and the resulting mixtures were analyzed. The concentration of the two hydrogel precursors with respect to the liquid phase was the same as those investigated for the CPC composites (i.e., DGL/PEG-NHS = 8/50, 16/100, 24/150, or 40/250 mg ml^{-1}). As expected, a variation of the tangent of the phase angle was observed when the mixtures evolved from a liquid state to an elastomer state, once the reticulation of the hydrogel has occurred (Figure 3 and Figure S2).

The time elapsed at the beginning (~ 60 s) and at the end (300–900 s) of this variation is reported in Table 2, giving an indication on the time range for the formation of the hydrogel network, in the absence of the CPC powder.

DGL/PEG-NHS (mg ml ⁻¹)	t ₁ (ε') (min)	t ₁ (ε'') (min)	t ₂ (ε') (min)	t ₂ (ε'') (min)
Liquid phase: 5 wt.% Na ₂ HPO ₄				
0/0	20 ± 1	15 ± 1	38 ± 2	39 ± 2
16/100	30 ± 2	23 ± 1	66 ± 3	70 ± 3
24/150	30 ± 2	19 ± 1	93 ± 2	107 ± 4
Liquid phase: 2 wt.% Na ₂ HPO ₄				
0/0	60 ± 2	60 ± 2	95 ± 2	105 ± 3
16/100	160 ± 6	130 ± 5	260 ± 10	300 ± 4
24/150	295 ± 6	275 ± 8	430 ± 10	465 ± 14
40/250	375 ± 8	375 ± 5	520 ± 9	590 ± 5

TABLE 1 Characteristic parameters resulting from the monitoring of the setting reaction of the HBS-0 reference cement and the corresponding composites at 37°C, using high-frequency impedance measurements

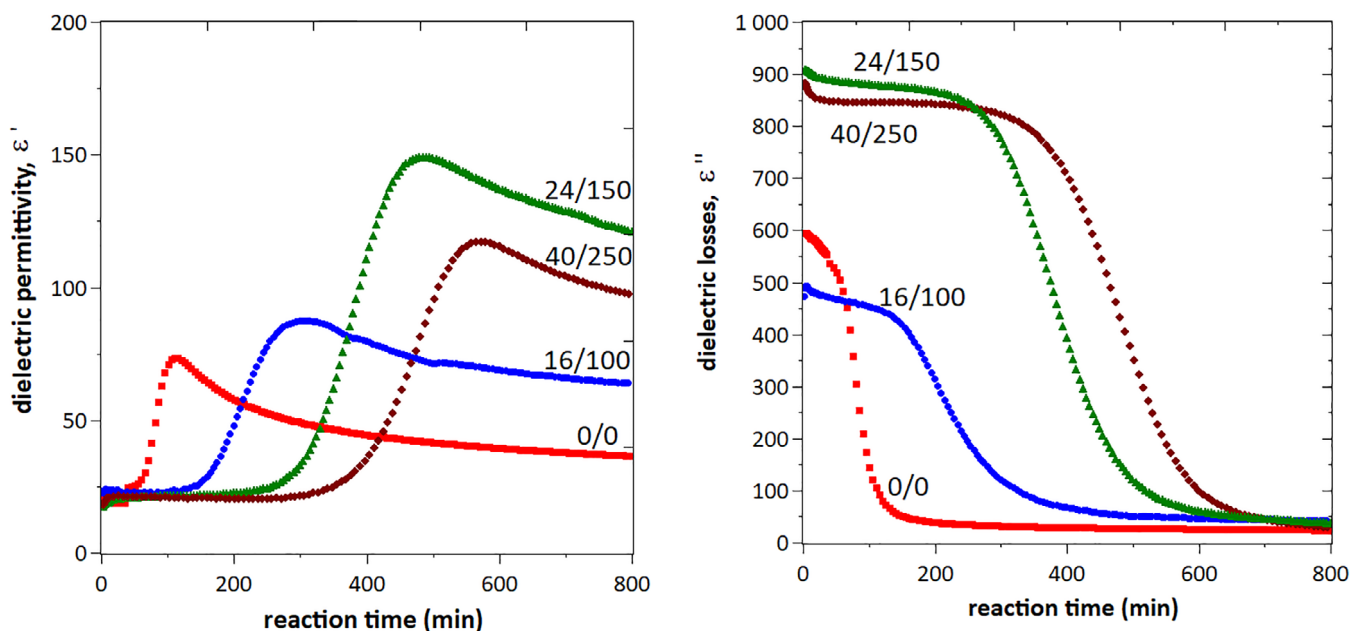


FIGURE 2 Variation of dielectric permittivity, ε' (left), and dielectric losses, ε'' (right), versus reaction time for the HBS-0 reference (0/0) and the calcium phosphate cement (CPC) composites loaded with poly(L-lysine) dendrigraft (DGL)/polyethylene glycol homobifunctionalized with N-hydroxysuccinimide (PEG-NHS): respectively, 16 mg ml⁻¹/100 mg ml⁻¹, 24 mg ml⁻¹/150 mg ml⁻¹, and 40 mg ml⁻¹/250 mg ml⁻¹, with a 2 wt.% Na₂HPO₄ liquid phase. Frequency: 10 MHz, 37°C

The usual way to assess the initial and final setting time of CPC is the use of the Gillmore needles standard test method, by measuring the change in the material's penetration resistance. However, in the present case, the reticulation of the organic polymer most often conferred an elastic character to the cement paste, which made indentation hardly observable. Hence, the Gillmore needles method was not appropriate for the present study. For this reason, DMA experiments were used to monitor the setting of the CPC composites by comparison with the HBS-0 references. For the two references, the CPC powder was mixed with the aqueous disodium phosphate solution (2 or 5 wt.%) for 1 min, and the resulting paste was then analyzed by DMA. For the composites, the same procedure was carried out, that is, the DGL solution was added to the HBS-0 powder combined with PEG-NHS, and after mixing (1 min), the resulting cement paste was analyzed (Figures S3 and S4). Figure 4 shows typical DMA curves, obtained for the HBS-0 cement reference and the 24/150 composite both prepared using a

5 wt.% aqueous Na₂HPO₄ solution. A progressive increase of tan δ was observed during the first 20 min for the CPC reference, giving evidence of a gradual thickening of the cement paste as the cement setting reaction takes place (i.e., precipitation of apatite crystals in the intergranular space). A maximum was then reached and the signal became erratic until a sharp return to the baseline, as a consequence of the cement rigidification. When the hydrogel precursors were added to the cement, similar profiles were observed. However, a low decrease of tan δ was observed during the first 12 min, possibly due to a higher fluidity of the cement paste caused by the presence of the hydrogel precursors. Then a linear increase was observed, linked to the concomitant reticulation of the hydrogel and cement setting reaction, followed by a longer erratic plateau before returning to baseline. The time elapsed for these three particular events are reported in Table 3.

By contrast, when the phosphate concentration in the liquid phase was lower (i.e., 2 wt.% Na₂HPO₄), the variation of tan δ

started significantly later for the HBS-0 reference since the setting reaction was delayed in these conditions (Figure S3). Interestingly, the variation of $\tan \delta$ started earlier in the case of the CPC composites, as a result of the rapid hydrogel formation that occurred faster than the precipitation of apatite in the intergranular space.

From a clinical perspective, it was important to determine how long molding/shaping is possible and when surgical closure of the wound might be initiated when using this type of CPC composite. Interestingly, while the Gillmore needles method was not appropriate for this purpose, this information can be assessed from the DMA measurements. Indeed, the time elapsed at the end of the increase of the $\tan \delta$ can be considered as the limit value that should not be exceeded for manipulating the CPC composites. On the other hand, the time elapsed for the $\tan \delta$ to return to the baseline corresponds to the complete rigidification of the material. In the case of the 8/50, 16/100, and 24/150 CPC composites prepared in 2 wt.% Na_2HPO_4 , these two characteristic values (15–20 and 38–47 min, respectively) were found to be in the same range than for the HBS reference (5 wt.

% Na_2HPO_4) which is currently used in clinics (17 and 31 min, respectively).

3.4 | Characterization of the microstructural and mechanical properties of the CPC composites

In order to investigate whether a 3D organic hydrogel network has formed in the different CPC composites, molded cylindrical cement blocks (setting time: 1 week) were immersed in a 10 wt.% solution of EDTA for 2 weeks. The reaction with EDTA specifically resulted in the full dissolution of the calcium phosphate component. When present, the organic component remaining after the decalcification process was submitted to successive washings to finish with a supercritical drying step using carbon dioxide to allow observation of the samples by SEM. Results about the decalcification experiments are summarized in Table 4 for the different conditions, that is, the presence or absence of an organic residue, shape, and behavior of the residue (see Figure S5).

One important feature for the practical use of CPCs is their ability to reach an appropriate cohesion after a few minutes to ensure that

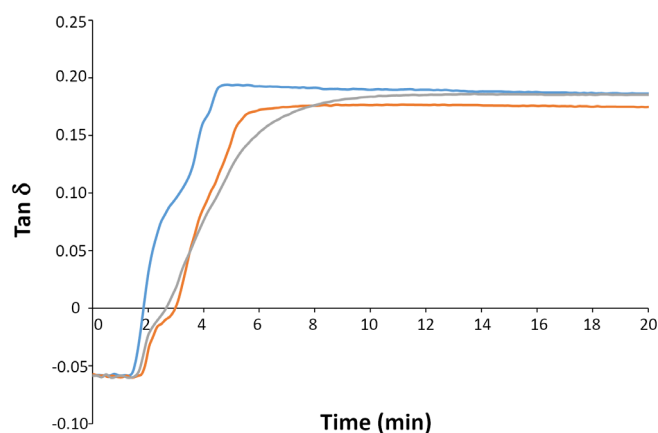


FIGURE 3 Variation of $\tan \delta$ versus time measured by dynamic mechanical analysis (DMA) on a poly(L-lysine) dendrigraft (DGL) solution (16 mg ml^{-1}) in 2 wt.% aqueous Na_2HPO_4 mixed with polyethylene glycol homobifunctionalized with N-hydroxysuccinimide (PEG-NHS) (100 mg ml^{-1}). The curves correspond to the repetition of three different experiments

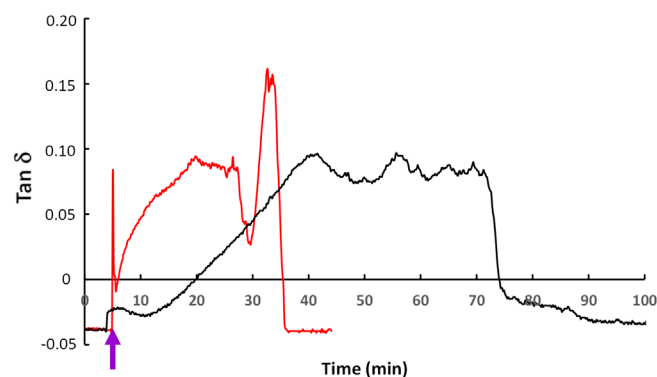


FIGURE 4 Variation of $\tan \delta$ versus time measured by dynamic mechanical analysis (DMA) on an HBS-0 reference (red line) and a 24/150 calcium phosphate cement (CPC) composite (black line), using a 5 wt.% Na_2HPO_4 liquid phase. The arrow indicates the time at which the sample was introduced in the DMA apparatus and the measurement was started

TABLE 2 Time elapsed for characteristic events of the variation of the tangent of the phase angle, for the DGL/PEG-NHS mixtures in 2 or 5 wt.% aqueous Na_2HPO_4

Liquid phase	5 wt.% Na_2HPO_4			2 wt.% Na_2HPO_4			
	8/50	16/100	24/150	8/50	16/100	24/150	40/250
DGL/PEG-NHS (mg ml^{-1})	8/50	16/100	24/150	8/50	16/100	24/150	40/250
Time elapsed at the beginning of the variation of the $\tan \delta$ (s)	96 ± 37^a	52 ± 2	60 ± 3	88 ± 13^b	53 ± 1	62 ± 9	57 ± 4
Time elapsed at the end of the variation of the $\tan \delta$ (s)	403 ± 128	857 ± 212^b	536 ± 14	765 ± 55^c	473 ± 187^d	841 ± 282^e	306 ± 64

^aSignificant difference between the DGL/PEG-NHS 8/50 and 16/100 hydrogels formed in 5 wt.% Na_2HPO_4 ($p < .05$).

^bStatistically significant difference between hydrogels for a given disodium phosphate concentration ($p < .05$).

^cSignificant difference between the DGL/PEG-NHS 8/50 and 40/250 hydrogels formed in 2 wt.% Na_2HPO_4 ($p < .05$).

^dSignificant difference between the DGL/PEG-NHS 16/100 and 24/150 hydrogels formed in 2 wt.% Na_2HPO_4 ($p < .05$).

^eSignificant difference between the DGL/PEG-NHS 24/150 and 40/250 hydrogels formed in 2 wt.% Na_2HPO_4 ($p < .05$).

TABLE 3 Time elapsed for characteristic events of the variation of the $\tan \delta$, for the calcium phosphate cement (CPC) composites compared to the CPC references, using a 2 or 5 wt.% aqueous Na_2HPO_4 solution

Liquid phase	5 wt.% Na_2HPO_4				2 wt.% Na_2HPO_4					
	DGL/PEG-NHS (mg ml ⁻¹)	0/0	8/50	16/100	24/150	0/0	8/50	16/100	24/150	40/250
Time elapsed at the beginning of the increase of the $\tan \delta$ (s)		121 ± 6	134 ± 1	624 ± 5 ^a	582 ± 28 ^b	1,112 ± 103 ^a	112 ± 65 ^c	291 ± 42	178 ± 35	174 ± 8
Time elapsed at the end of the increase of the $\tan \delta$ (s)		1,019 ± 93	1,096 ± 102	2,474 ± 21 ^a	2,110 ± 173 ^b	2,002 ± 241	1,334 ± 806	1,273 ± 326	891 ± 144 ^d	1,176 ± 88
Time elapsed for the $\tan \delta$ (s) to return to the baseline		1,844 ± 176	1963 ± 52	3,920 ± 125 ^a	4,256 ± 93 ^b	2,864 ± 479	2,265 ± 682	2,628 ± 572	2,836 ± 323	3,340 ± 131

^aStatistically significant difference between composites for a given disodium phosphate concentration ($p < .05$).

^bSignificant difference between the DGL/PEG-NHS 8/50 and 16/100 hydrogels formed in 5 wt.% Na_2HPO_4 ($p < .05$).

^cStatistically significant difference between the DGL/PEG-NHS 8/50 and 16/100 composites formed in 2 wt.% Na_2HPO_4 ($p < .05$).

^dStatistically significant difference between the DGL/PEG-NHS 24/150 composite and the cement reference formed in 2 wt.% Na_2HPO_4 ($p < .05$).

TABLE 4 General properties of the different calcium phosphate cement (CPC) composites and related HBS-0 references: injectability, compressive strength, and qualitative assessment of the organic component [only for the CPC composites]

	Liquid phase DGL/PEG-NHS (mg ml ⁻¹)	2 wt.% Na_2HPO_4			
		8/50	16/100	24/150	40/250
Decalcified samples	Presence of an organic residue	Yes	Yes	Yes	Yes
	Behavior of the residue in water	Shapeless, non-self supporting	Cylinder-shape, non-self supporting	Cylinder-shape, self supporting	Expanded cylinder-shape, self supporting
Compressive strength (MPa)		14.96 ± 1.18 ^a	14.32 ± 1.66 ^a	19.62 ± 1.19 ^a	15.16 ± 1.78 ^a
		12.68 ± 2.25 for HBS-0			
Amount of cement paste extruded after 15 min (applied extrusion force in N)		64% ± 1 (24 ± 4)	81% ± 3 (12 ± 3)	89% ± 1 (19 ± 2)	95% ± 1 (2 ± 1)
Amount of cement paste extruded after 15 min (applied extrusion force in N)		89% ± 1 (2 ± 0.3) for HBS-0			
	Liquid phase DGL/PEG-NHS (mg ml ⁻¹)	5 wt.% Na_2HPO_4			
		8/50		16/100	24/150
Decalcified samples	Presence of an organic residue	No		Yes	Yes
	Behavior of the residue in water	n/a		Shapeless, non-self supporting	Cylinder-shape, non-self supporting
Compressive strength (MPa)		15.2 ± 1.27		14.54 ± 0.78 ^b	16.86 ± 2.82 ^b
		18.79 ± 2.41 for HBS-0 13.18 ± 2.26 for HBS			
Amount of cement paste extruded after 15 min (applied extrusion force in N)		90% (7 ± 1)		95% (4 ± 1)	85% (41 ± 3)
Amount of cement paste extruded after 15 min (applied extrusion force in N)		74% ± 1 (12 ± 1) for HBS-0 93% ± 1 (17 ± 2) for HBS			

^aThe 8/50, 16/100, and 40/250 formulations were statistically significant different from the 24/150 formulation (p values $< .05$).

^b16/100 and 24/250 are statistically different, with p values in t test of .002 and .005, respectively.

no disaggregation of the cement paste will occur on the implantation site where bleeding often takes place. Hence, the cohesion of the different composites was studied by extrusion of the paste into a 0.9 wt

% NaCl solution at 37°C, 15 min after the preparation of the cement paste (see Figure S6). By contrast with the HBS-0 reference that was not cohesive in any of the tested conditions (i.e., using a 2 or 5 wt.%

aqueous Na_2HPO_4 solution as the CPC liquid phase), a correct to very good cohesion was observed for all the composites. In addition, while the 40/250 sample (2 wt.% aqueous Na_2HPO_4) was found to be very cohesive, swelling of the cement paste was observed as well.

The injectability of the cement pastes and their behavior under pressure was assessed using extrusion tests (Bohner & Baroud, 2005; Ginebra et al., 2001; Khairoun et al., 1998). After mixing the solid and liquid phases for 1 min, the different samples were put in a syringe and extruded at a constant rate 15 min after the paste preparation. Typically, the extrusion force rapidly reaches a plateau, followed by a very sharp increase, which corresponds either to the beginning of the hardening process or a filter-pressing phenomenon (i.e., phase segregation between the liquid and solid phases) or to a full injection of the paste. As shown in Table 4, only two conditions [40/250, 2 wt.% aqueous Na_2HPO_4 –16/100, 5 wt.% aqueous Na_2HPO_4] were found for which the full content of the syringe could be injected (>90%). In both cases the force to apply was very low when compared to the commercial HBS[®] reference and statistically different (*p* values were 0 in *t* test). Surprisingly, the compressive strengths (MPa) were in a similar range for all the series of composites.

SEM observations of polished cross-sections of the CPC composites were performed to compare their microstructure. When using a 5 wt.% aqueous Na_2HPO_4 solution as the liquid phase, different types

of particles can be observed for the polymer-free HBS-0 reference, the size of which is representative of the granulometry of the CPC powder (size distribution: 1.4–32 μm average size = 9 μm —Figure 5): (a) a small amount of those are dense, either along their whole cross-section or in their inner part, and correspond to unreacted or partially hydrolyzed α -TCP or DCPD; (b) a large amount of particles have a geode-like morphology with a dense shell lined in its inner part with interdigitated platelet crystals, as a result of full hydrolysis of α -TCP into CDA (Figure 6).

The area in between all these particles is mostly occupied by CDA platelet crystals forming channels with a “sand rose” architecture, having a typical width of \sim 1–3 μm . No significant change in the microstructure was observed when increasing amounts of DGL and PEH-NHS (8/50, 16/100, and 24/150 CPC composites) were introduced in the formulation (see Figure 6). When using a 2 wt.% aqueous Na_2HPO_4 solution as the liquid phase, a similar microstructure was also present for the polymer-free HBS-0 reference (Figure 7). However, the addition of DGL and PEH-NHS led to a significant modification of the microstructure, in particular for the 24/150 and 40/250 CPC composites (Figure 8): first, a decrease of the size of the transformed α -TCP particles has occurred and their morphology has changed as well. Hence, it becomes more difficult to differentiate them from the network of

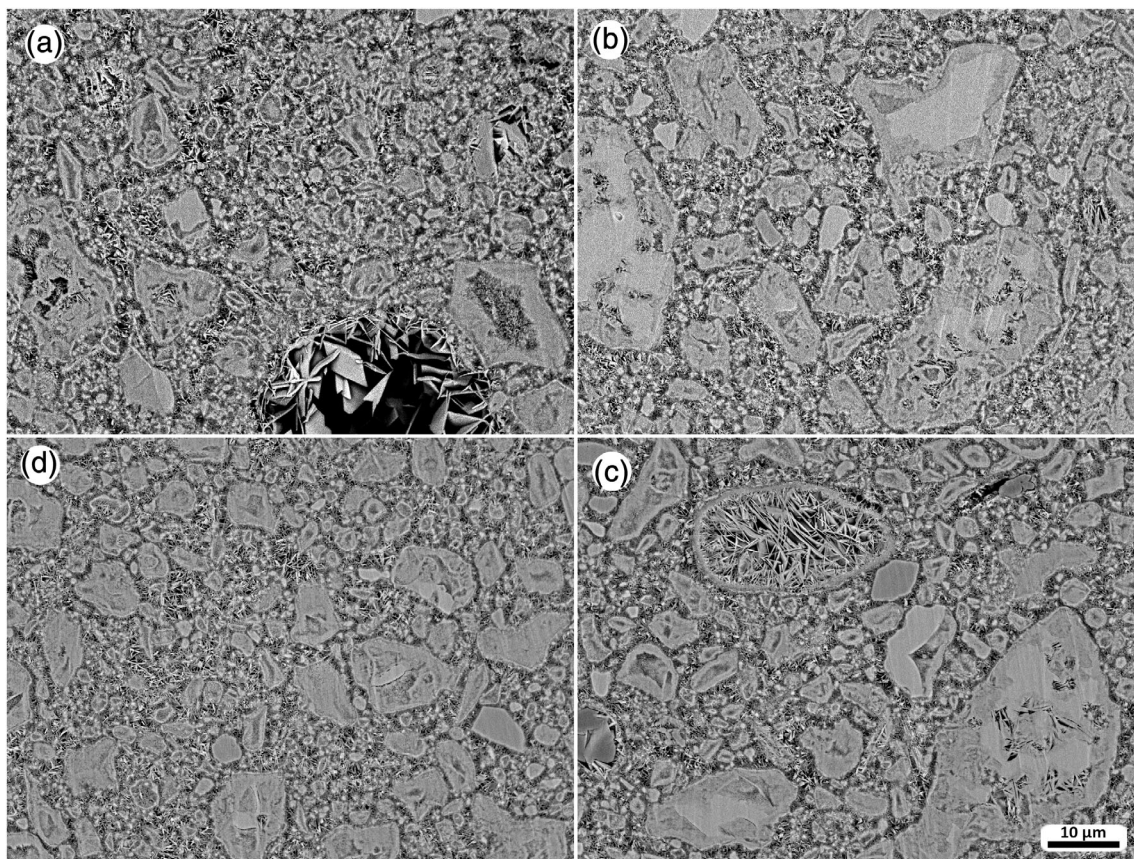


FIGURE 5 Scanning electron microscopy (SEM) observation of a polished cross-section of the HBS-0 reference (a) and the 8/50 (b), 16/100 (c), and 24/150 (d) calcium phosphate cement (CPC) composites, using a 5 wt.% aqueous Na_2HPO_4 solution as a liquid phase, after a setting time of 1 week. Magnification: \times 1,500

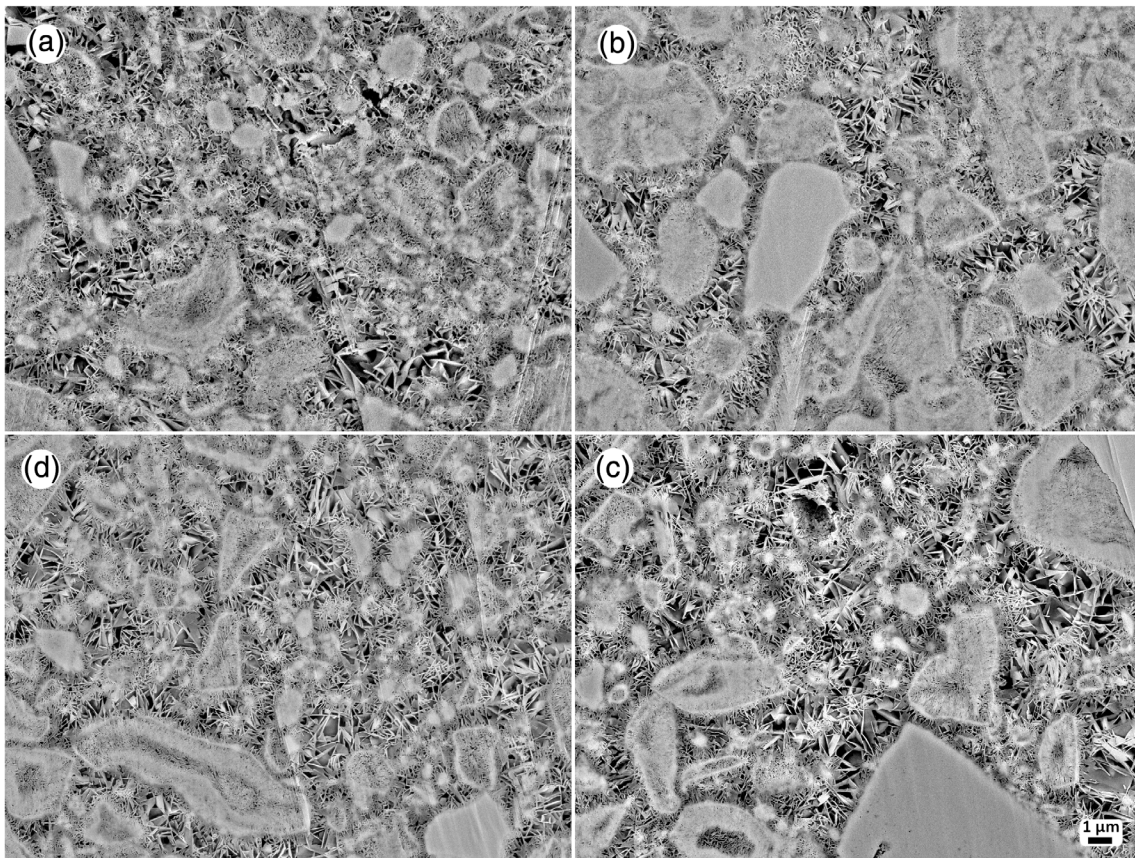


FIGURE 6 Scanning electron microscopy (SEM) observation of a polished cross-section of the HBS-0 reference (a) and the 8/50 (b), 16/100 (c), and 24/150 (d) CPC composites, using a 5 wt.% aqueous Na_2HPO_4 solution as a liquid phase, after a setting time of 1 week. Magnification: $\times 5,000$

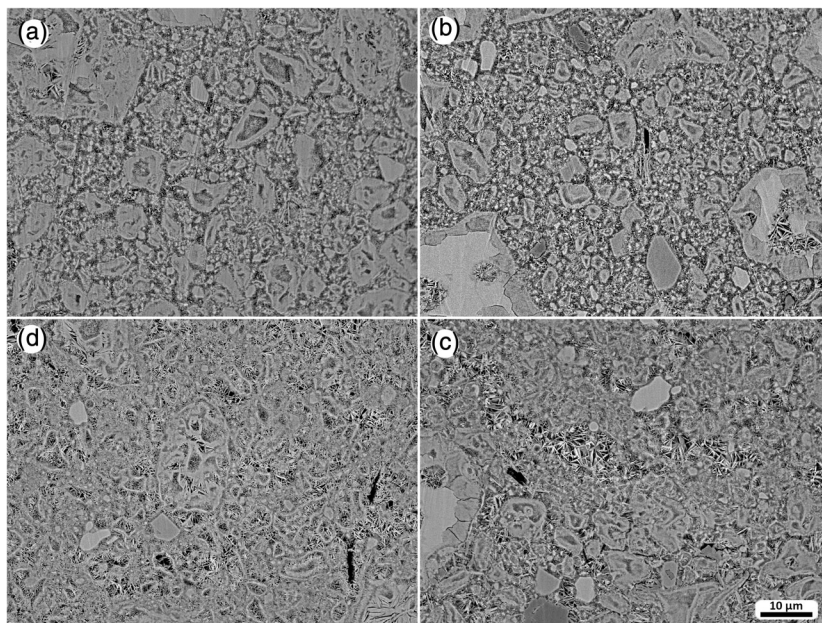


FIGURE 7 Scanning electron microscopy (SEM) observation of a polished cross-section of the HBS-0 reference (a) and the 16/100 (b), 24/150 (c), and 40/250 (d) calcium phosphate cement (CPC) composites, using a 2 wt.% aqueous Na_2HPO_4 solution as a liquid phase, after a setting time of 1 week. Magnification: $\times 1,500$

platelet crystals present in the intergranular space, the size of which is significantly larger in some places, when compared to the CPC reference.

In order to characterize the organic component present in the CPC composites, SEM observations of a fracture plane of the decalcified samples were also performed. Images of the decalcified

FIGURE 8 Scanning electron microscopy (SEM) observation of a polished cross-section of the HBS-0 reference (a) and the 16/100 (b), 24/150 (c), and 40/250 (d) calcium phosphate cement (CPC) composites, using a 2 wt.% aqueous Na_2HPO_4 solution as a liquid phase, after a setting time of 1 week. Magnification: $\times 5,000$

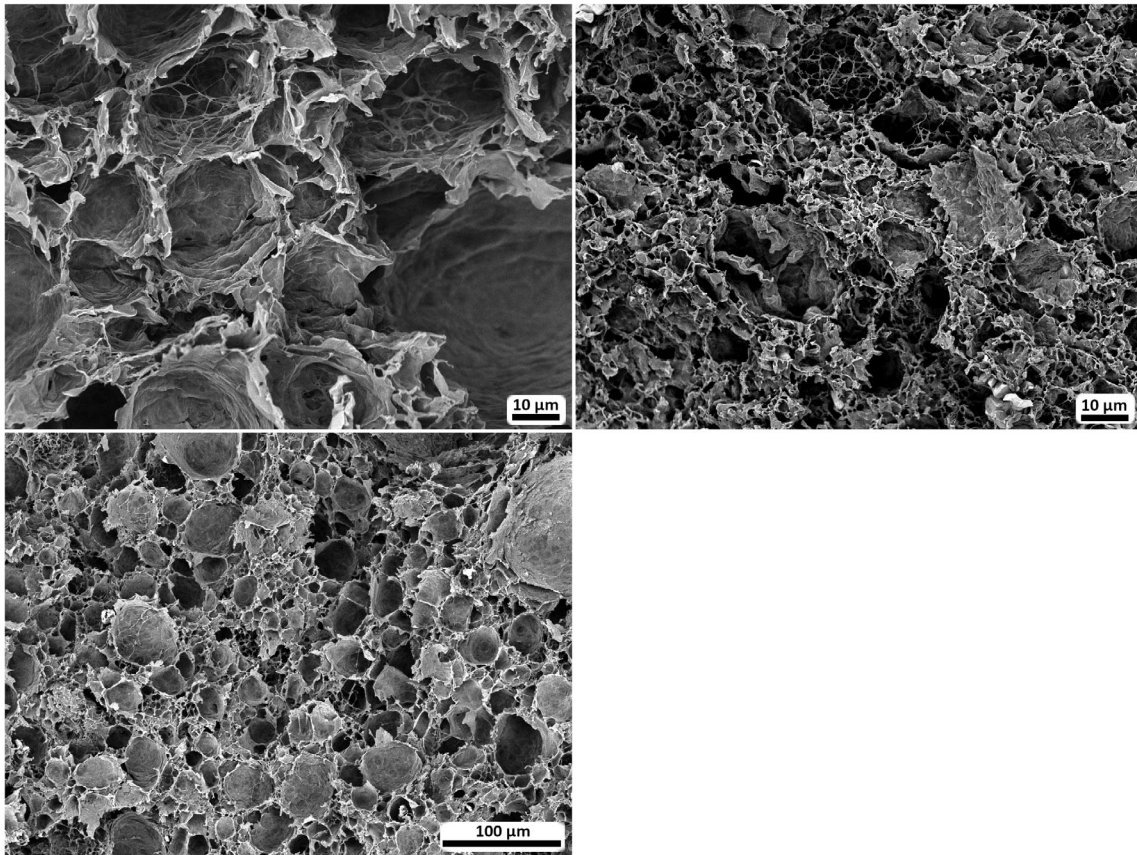
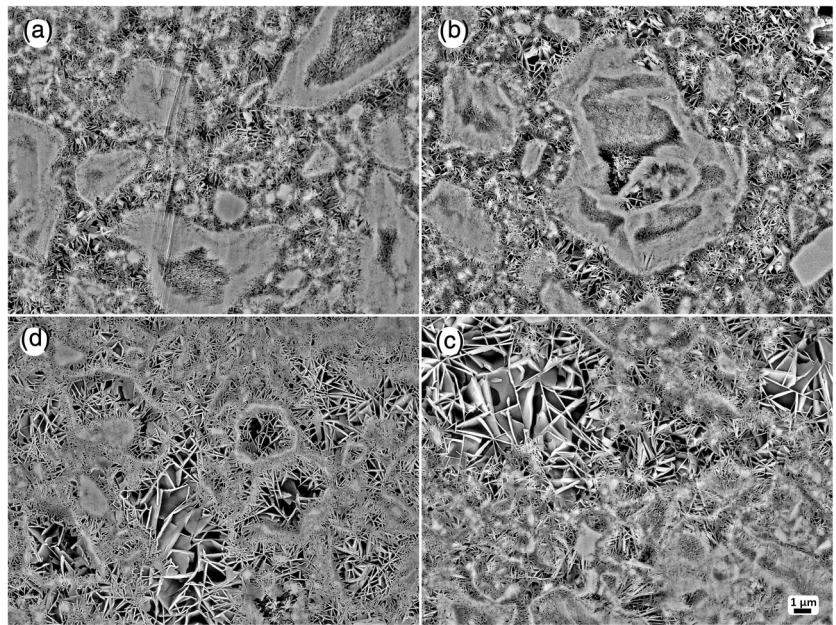


FIGURE 9 Scanning electron microscopy (SEM) observation of a fracture plane of calcium phosphate cement (CPC) composites (liquid phase: 2 wt.% aqueous Na_2HPO_4 solution) after EDTA-mediated removal of the inorganic component. Right view: 24/150 CPC composite (magnification: $\times 1,000$). Left views: 40/250 CPC composite (magnification: $\times 1,000$ (top); $\times 250$ (bottom))

24/150 and 40/250 CPC composites (liquid phase: 2 wt.% aqueous Na_2HPO_4 solution) are presented in Figure 9, showing that the continuous 3D organic network present in the two materials is highly porous and corresponds to the negative imprint of apatite crystals formed

during the setting process. The main difference between the two samples lies in the fact that the polymer scaffold formed in the 40/250 CPC composite was rigid enough to retain its shape after the dissolution of the calcium phosphate component and supercritical drying. By

contrast, an important shrinkage was observed for the 24/150 sample during the drying process.

4 | DISCUSSION

The main objective of this study was to investigate to which extent the general properties of an injectable apatitic cement might be affected when introducing in the cement formulation synthetic precursors that would self-assemble to form a biocompatible hydrogel once the CPC solid and liquid phases are mixed. Indeed, the formation of a 3D continuous organic network in the intergranular space might alter the precipitation and crystal growth of apatite, which is the driving force of the cement setting reaction.

For that purpose, two reagents capable to form a biocompatible hydrogel in a few minutes were introduced into a polymer-free CPC formulation (HBS-0): a 10 kDa polyethylene glycol chain end-capped with two N-hydroxysuccinimide groups (noted PEG-NHS) that was mixed to the solid phase of the CPC, and a third-generation cross-linked dendrimer grafted with lysine end-groups (noted DGL) (Collet et al., 2010) which was dissolved in the liquid phase. While the relative DGL/PEG-NHS weight ratio was kept constant (0.16), the total amount of the two precursors introduced in the CPC formulation was allowed to vary. Limited solubility of the PEG-NHS component was noted when using the normal liquid phase for Graftys HBS (i.e., 5 wt.% aqueous Na_2HPO_4) and for this reason, a less concentrated solution (2 wt.% aqueous Na_2HPO_4) was also investigated in this work, to allow a higher loading of the hydrogel precursors.

For the two liquid phases, conditions similar to the preparation of the cement paste were used to assess the kinetics of the formation of the hydrogel in the absence of the CPC powder. On the basis of dynamic mechanical analyses, the transition from the liquid to hydrogel state started after ~ 1 min and ended after about 4–14 min, depending on the liquid phase and amount of hydrogel precursors. On the other hand, high-frequency impedance measurements showed that in the case of the 5 wt.% aqueous Na_2HPO_4 solution, the precipitation of apatite crystals was found to occur in the same time range than the hydrogel formation. By comparison with the polymer-free HBS-0 reference, the end of the inorganic network formation was shifted toward longer times in direct proportion with the amount of hydrogel precursors loaded in the cement composition (i.e., ~ 40 min for 0/0, 70 min for 16/100, and 100 min for 24/150—Figure S1). The same trend was observed using DMA, since the higher the content in hydrogel precursors, the longer the time before rigidification of the cement paste (i.e., ~ 30 min for 0/0, 33 min for 8/50, 65 min for 16/100, and 71 min for 24/150—see Table 3). Finally, no significant change in the microstructure was observed upon the addition of PEG-NHS and DGL in the CPC formulation (Figures 5 and 6). These results altogether suggest that the concomitant formation of the organic and inorganic networks affects both reactions since (a) either no hydrogel (8/50) or a poorly reticulated organic network was formed (16/100 and 24/150), as evidenced by the decalcification experiments; (b) the kinetic of the setting reaction driven by the precipitation of apatite

crystals in the intergranular structure was slowed down, as the amount of hydrogel precursors was increased. Moreover, for the three composites, the compressive strengths (MPa) were in the same range. While the cohesion and injectability of the HBS-0 reference were insufficient (Table 4), the three composites showed, however, a very good cohesion 15 min after preparation of the cement paste, and the injectability was also found to be correct, except for the 24/150 composite for which the force needed for extrusion was very high (~ 40 N). All CPC composite samples exhibited a statistically significant difference from HBS-0 reference and between them (p values were ~ 0 in t test). In summary, while the commercial Graftys HBS cement contains 2 wt.% HPMC to provide suitable cohesion and injectability, similar performances were obtained with DGL/PEG-NHS for the 8/50 and 16/100 composites.

By contrast, the use of a 2 wt.% aqueous Na_2HPO_4 solution resulted in a slower supersaturation of the liquid phase with calcium and phosphate ions, so that the cement setting reaction was delayed by 1 hr for the HBS-0 reference (Figure 2). Therefore, the formation of the hydrogel took place prior to the apatite precipitation, and the presence of a 3D organic network was evidenced for the four composites thanks to the decalcification experiments (Table 4). In the case of the 24/150 and 40/250 composites, the density of the hydrogel was found to be high enough to allow the material to self-support in water once the inorganic network has been removed. Interestingly, after decalcification of the 40/250 composite, the size of the hydrogel was even found to have expanded by $\sim 15\%$ in water with respect with the initial size of the hardened cement block and these dimensions were also preserved after drying, by contrast with the other composites for which a shrinkage of $\sim 55\%$ was observed when dried using supercritical carbon dioxide.

Due to the rapid formation of the hydrogel in the intergranular space, the setting reaction was therefore hampered, as confirmed by the high-frequency impedance and DMA measurements showing that the formation of the inorganic network was even more delayed when increasing the amounts of DGL and PEG-NHS introduced in the CPC formulation. In terms of cohesion, all the composites were cohesive. As regards the injectability, filter-pressing was present for the 8/50 and 16/100 composites, while the injectability was found to be excellent for the 40/250 sample, for which the totality of the paste could be extruded and the force to apply was very low, giving evidence of the high fluidity of this material. All the CPC composites exhibited a statistically significant difference from the HBS-0 reference and between them (p values were ~ 0 in t test).

Once hardened, in particular for the 24/150 and 40/250 CPC composites, the observed microstructure significantly differed from that of the HBS-0 reference (Figures 7 and 8). First, the size of the transformed α -TCP particles was smaller. Normally, the hydrolysis of the α -TCP particles results in (a) the concomitant precipitation of apatite needles on their surface with the formation of a dense shell (Figure 8a) and their size once transformed does not change much; (b) the precipitation of CDA platelet crystals with a “sand rose” architecture in the intergranular space. By contrast, in the case of the 24/150 and 40/250 CPC composites, likely because the α -TCP particles were

embedded in the 3D organic network before the setting reaction started, the dissolution of α -TCP mainly results in the precipitation of platelet crystals within the porous polymer scaffold (Figure 8d). Moreover, the size of the apatite crystals was significantly larger at some places, when compared to the CPC reference, as a result of a probable confinement effect that leads to a slower crystal growth. Finally, no significant improvement was again observed in terms of compressive strength (MPa) upon the addition of PEG-NHS and DGL in the CPC formulation. However, while the fracture of the polymer-free HBS-0 reference led to the formation of a large amount of small debris due to its brittle character, compression of the CPC composites led to deformation and crushing of the samples as a result of the embedment of the apatite crystals in the organic network, with a generation of a very limited amount of small debris.

5 | CONCLUSION

The introduction of polymers in CPCs is a common strategy to make them injectable and improve their cohesion, but at the end, the polymer is simply trapped in the CPC structure and no organic subnetwork is present. In the present study, organic monomers were combined to a CPC and conditions were found to make them reticulate in situ to form a biocompatible 3D polymeric scaffold in the intergranular space, before the growth of the apatitic inorganic network had started. Hence, the precipitation of apatite occurred within the porous polymer network, and the organic component was shown to strongly affect the size, density, and arrangement of the apatite crystals formed during the setting reaction, thereby leading to an original microstructure. From a clinical perspective, some of the composites reported here were found to be similar to clinically used CPCs, in terms of cohesion and setting time, with an even better injectability. Moreover, given that the polymer formed in the CPC was previously shown to be noncytotoxic and to act as a support promoting cellular attachment and proliferation, while being biocompatible and degraded in vivo through phagocytosis by macrophages, it might offer great potential in the context of bone regeneration and repair. Finally, the presence of this hydrophilic polymeric subnetwork in the composites might confer a higher permeability to the CPC. It would thus be of great interest to investigate whether this change in the microstructure might result in a different in vivo behavior, in terms of resorption rate when implanted in bone defects.

Another potential interest is the opportunity offered by the aqueous environment used to crosslink the DGL and PEG-NHS to entrap water-soluble compounds in the hydrogel. For instance, the incorporation of a recombinant elastin-derived protein was shown to enhance the elastic modulus of the resulting hydrogels (Debret et al., 2017) and this might be an attractive strategy to further improve the mechanical properties of these CPC composites.

ACKNOWLEDGMENTS

This work was partially supported by BPI-France (23rd call for R&D proposals of FUI - grant DOS0056563/00—SpineFlex project) and

the COLCOM and Graftys companies. The authors greatly acknowledge the Scanning Electron Microscopy facility at the Institut des Matériaux Jean Rouxel (IMN) laboratory, and particularly Nicolas Stephant for his technical support. The authors greatly acknowledge Nathalie Guichard from the CEISAM laboratory for his help for the data acquisition related to injectability, cohesion, and mechanical properties.

CONFLICT OF INTEREST

Some authors of this publication have research support from Graftys SA. The terms of this arrangement have been reviewed and approved by both CNRS and the University of Nantes in accordance with their policy on objectivity in research.

ORCID

Bruno Bujoli  <https://orcid.org/0000-0002-2256-0792>

REFERENCES

- Alkhraisat, M. H., Rueda, C., Marino, F. T., Torres, J., Jerez, L. B., Gbureck, U., & Cabarcos, E. L. (2009). The effect of hyaluronic acid on brushite cement cohesion. *Acta Biomaterialia*, 5, 3150–3156.
- Bajammal, S. S., Zlowodzki, M., Lelwica, A., Tornetta, P., Einhorn, T. A., Buckley, R., ... Bhandari, M. (2008). The use of calcium phosphate bone cement in fracture treatment. *The Journal of Bone and Joint Surgery American Volume*, 90A, 1186–1196.
- Bohner, M., & Baroud, G. (2005). Injectability of calcium phosphate pastes. *Biomaterials*, 26, 1553–1563.
- Bohner, M., Doebelin, N., & Baroud, G. (2006). Theoretical and experimental approach to test the cohesion of calcium phosphate pastes. *European Cells & Materials*, 12, 26–35.
- Bohner, M., Gbureck, U., & Barralet, J. E. (2005). Technological issues for the development of more efficient calcium phosphate bone cements: A critical assessment. *Biomaterials*, 26, 6423–6429.
- Brown, W. E., & Chow, L. C. (1983). A new calcium phosphate setting cement. *Journal of Dental Research*, 62, 672–679.
- Burguera, E. F., Xu, H. H. K., & Weir, M. D. (2006). Injectable and rapid-setting calcium phosphate bone cement with dicalcium phosphate dihydrate. *Journal of Biomedical Materials Research, Part B: Applied Biomaterials*, 77B, 126–134.
- Carey, L. E., Xu, H. H. K., Simon, C. G., Takagi, S., & Chow, L. C. (2005). Premixed rapid-setting calcium phosphate composites for bone repair. *Biomaterials*, 26, 5002–5014.
- Chen, G., Li, W., Yu, X., & Sun, K. (2009). Study of the cohesion of TTCP/DCPA phosphate cement through evolution of cohesion time and remaining percentage. *Journal of Materials Science*, 44, 828–834.
- Cherng, A., Takagi, S., & Chow, L. C. (1997). Effects of hydroxypropyl methylcellulose and other gelling agents on the handling properties of calcium phosphate cement. *Journal of Biomedical Materials Research*, 35, 273–277.
- Collet, H., Souaid, E., Cottet, H., Deratani, A., Boiteau, L., Dessalces, G., ... Pascal, R. (2010). An expeditious multigram-scale synthesis of lysine dendrigraft (DGL) polymers by aqueous N-carboxyanhydride polycondensation. *Chemistry*, 16, 2309–2316.
- Debret, R., Faye, C., Sohier, J., & Sommer P. (2017). Applicants: CNRS and Université Claude Bernard Lyon 1, International Patent No. WO2017194761.
- del Real, R. P., Ooms, E., Wolke, J. G. C., Vallet-Regi, M., & Jansen, J. A. (2003). In vivo bone response to porous calcium phosphate cement. *Journal of Biomedical Materials Research Part A*, 65A, 30–36.

- Despas, C., Schnitzler, V., Janvier, P., Fayon, F., Massiot, D., Bouler, J. M., ... Walcarius, A. (2014). High-frequency impedance measurement as a relevant tool for monitoring the apatitic cement setting reaction. *Acta Biomaterialia*, 10, 940–950.
- Dorozhkin, S. V. (2008). Calcium orthophosphate cements for biomedical application. *Journal of Materials Science*, 43, 3028–3057.
- Dorozhkin, S. V. (2013). Self-setting calcium orthophosphate formulations. *Journal of Functional Biomaterials*, 4, 209–311.
- Drury, J. L., & Mooney, D. J. (2003). Hydrogels for tissue engineering: Scaffold design variables and applications. *Biomaterials*, 24, 4337–4351.
- Fernandez, E., Gil, F. J., Best, S. M., Ginebra, M. P., Driessens, F. C. M., & Planell, J. A. (1998). Improvement of the mechanical properties of new calcium phosphate bone cements in the CaHPO₄-alpha-Ca₃(PO₄)₂ system: Compressive strength and microstructural development. *Journal of Biomedical Materials Research*, 41, 560–567.
- Francoia, J.-P., & Vial, L. (2018). Everything you always wanted to know about poly-L-lysine dendrigrafts (but were afraid to ask). *Chemistry*, 24, 2806–2814.
- Gauthier, O., Bouler, J. M., Aguado, E., Pilet, P., & Daculsi, G. (1998). Macroporous biphasic calcium phosphate ceramics: Influence of macropore diameter and macroporosity percentage on bone ingrowth. *Biomaterials*, 19, 133–139.
- Ginebra, M. P., Espanol, M., Montufar, E. B., Perez, R. A., & Mestres, G. (2010). New processing approaches in calcium phosphate cements and their applications in regenerative medicine. *Acta Biomaterialia*, 6, 2863–2873.
- Ginebra, M. P., Rilliard, A., Fernandez, E., Elvira, C., San Roman, J., & Planell, J. A. (2001). Mechanical and rheological improvement of a calcium phosphate cement by the addition of a polymeric drug. *Journal of Biomedical Materials Research*, 57, 113–118.
- Habib, M., Baroud, G., Gitzhofer, F., & Bohner, M. (2008). Mechanisms underlying the limited injectability of hydraulic calcium phosphate paste. *Acta Biomaterialia*, 4, 1465–1471.
- Ishikawa, K., Miyamoto, Y., Kon, M., Nagayama, M., & Asaoka, K. (1995). Non-decay type fast-setting calcium-phosphate cement - composite with sodium alginate. *Biomaterials*, 16, 527–532.
- Johnson, A. J. W., & Herschler, B. A. (2011). A review of the mechanical behavior of CaP and CaP/polymer composites for applications in bone replacement and repair. *Acta Biomaterialia*, 7, 16–30.
- Jyoti, M. A., Thai, V. V., Min, Y. K., Lee, B.-T., & Song, H.-Y. (2010). In vitro bioactivity and biocompatibility of calcium phosphate cements using Hydroxy-propyl-methyl-cellulose (HPMC). *Applied Surface Science*, 257, 1533–1539.
- Khairoun, I., Boltong, M. G., Driessens, F. C. M., & Planell, J. A. (1998). Some factors controlling the injectability of calcium phosphate bone cements. *Journal of Materials Science Materials in Medicine*, 9, 425–428.
- Khairoun, I., Driessens, F. C. M., Boltong, M. G., Planell, J. A., & Wenz, R. (1999). Addition of cohesion promoters to calcium phosphate cements. *Biomaterials*, 20, 393–398.
- Khairoun, I., Magne, D., Gauthier, O., Bouler, J. M., Aguado, E., Daculsi, G., & Weiss, P. (2002). In vitro characterization and in vivo properties of a carbonated apatite bone cement. *Journal of Biomedical Materials Research*, 60, 633–642.
- Larsson, S., & Bauer, T. W. (2002). Use of injectable calcium phosphate cement for fracture fixation: A review. *Clinical Orthopaedics and Related Research*, 395, 23–32.
- Larsson, S., & Hannink, G. (2011). Injectable bone-graft substitutes: Current products, their characteristics and indications, and new developments. *Injury*, 42, S30–S34.
- LeGeros, R., Chohayeb, A., & Shulman, A. (1982). Apatitic calcium phosphates: Possible restorative materials. *Journal of Dental Research*, 61, 343.
- Lin, J. P., Zhang, S. N., Chen, T., Liu, C. S., Lin, S. L., & Tian, X. H. (2006). Calcium phosphate cement reinforced by polypeptide copolymers. *Journal of Biomedical Materials Research, Part B: Applied Biomaterials*, 76B, 432–439.
- Liu, H., Li, H., Cheng, W. J., Yang, Y., Zhu, M. Y., & Zhou, C. R. (2006). Novel injectable calcium phosphate/chitosan composites for bone substitute materials. *Acta Biomaterialia*, 2, 557–565.
- Liu, W., Zhang, J., Rethore, G., Khairoun, K., Pilet, P., Tancret, F., ... Weiss, P. (2014). A novel injectable, cohesive and toughened Si-HPMC (silanized-hydroxypropyl methylcellulose) composite calcium phosphate cement for bone substitution. *Acta Biomaterialia*, 10, 3335–3345.
- Liu, W., Zhang, J., Weiss, P., Tancret, F., & Bouler, J.-M. (2013). The influence of different cellulose ethers on both the handling and mechanical properties of calcium phosphate cements for bone substitution. *Acta Biomaterialia*, 9, 5740–5750.
- Lorion, C., Faye, C., Maret, B., Trimaille, T., Régnier, T., Sommer, P., & Debret, R. (2014). Biosynthetic support based on dendritic poly(L-lysine) improves human skin fibroblasts attachment. *Journal of Biomaterials Science-Polymer Edition*, 25, 136–149.
- Mirtchi, A. A., Lemaître, J., & Terao, N. (1989). Calcium-phosphate cements - Study of the beta-tricalcium phosphate - Monocalcium phosphate system. *Biomaterials*, 10, 475–480.
- Miyamoto, Y., Ishikawa, K., Takechi, M., Toh, T., Yuasa, T., Nagayama, M., & Suzuki, K. (1998). Basic properties of calcium phosphate cement containing atelocollagen in its liquid or powder phases. *Biomaterials*, 19, 707–715.
- O'Neill, R., McCarthy, H. O., Montufar, E. B., Ginebra, M.-P., Wilson, D. I., Lennon, A., & Dunne, N. (2017). Critical review: Injectability of calcium phosphate pastes and cements. *Acta Biomaterialia*, 50, 1–19.
- Romestand, B., Rolland, J.-L., Commeyras, A., Coussot, G., Desvignes, I., Pascal, R., & Vandenabeele-Trambouze, O. (2010). Dendrigraft poly-L-lysine: A non-immunogenic synthetic carrier for antibody production. *Biomacromolecules*, 11, 1169–1173.
- Song, H.-Y., Rahman, A. H. M. E., & Lee, B.-T. (2009). Fabrication of calcium phosphate-calcium sulfate injectable bone substitute using chitosan and citric acid. *Journal of Materials Science. Materials in Medicine*, 20, 935–941.
- Tajima, S., Nishimoto, N., Kishi, Y., Matsuya, S., & Ishikawa, K. (2004). Effects of added sodium alginate on mechanical strength of apatite cement. *Dental Materials Journal*, 23, 329–334.
- Takagi, S., Chow, L. C., Hirayama, S., & Eichmiller, F. C. (2003). Properties of elastomeric calcium phosphate cement-chitosan composites. *Dental Materials*, 19, 797–804.
- Thai, V. V., & Lee, B.-T. (2010). Fabrication of calcium phosphate-calcium sulfate injectable bone substitute using hydroxy-propyl-methyl-cellulose and citric acid. *Journal of Materials Science Materials in Medicine*, 21, 1867–1874.
- Thiebaut, J. M., Roussy, G., Chlihi, K., & Bessiere, J. (1989). Dielectric study of the activation of blende with cupric ions. *Journal of Electroanalytical Chemistry*, 262, 131–144.
- Wang, X., Chen, L., Xiang, H., & Ye, J. (2007). Influence of anti-washout agents on the rheological properties and injectability of a calcium phosphate cement. *Journal of Biomedical Materials Research, Part B: Applied Biomaterials*, 81B, 410–418.
- Xu, H. H. K., & Simon, C. G. (2005). Fast setting calcium phosphate-chitosan scaffold: Mechanical properties and biocompatibility. *Biomaterials*, 26, 1337–1348.
- Xu, H. H. K., Takagi, S., Quinn, J. B., & Chow, L. C. (2004). Fast-setting calcium phosphate scaffolds with tailored macropore formation rates for bone regeneration. *Journal of Biomedical Materials Research, Part A*, 68A, 725–734.
- Zhang, J., Liu, W., Gauthier, O., Sourice, S., Pilet, P., Rethore, G., ... Weiss, P. (2016). A simple and effective approach to prepare injectable macroporous calcium phosphate cement for bone repair: Syringe-foaming using a viscous hydrophilic polymeric solution. *Acta Biomaterialia*, 31, 326–338.
- Zhang, J., Liu, W., Schnitzler, V., Tancret, F., & Bouler, J.-M. (2014). Calcium phosphate cements for bone substitution: Chemistry, handling and mechanical properties. *Acta Biomaterialia*, 10, 1035–1049.

Zhang, J. T., Tancret, F., & Bouler, J. M. (2011). Fabrication and mechanical properties of calcium phosphate cements (CPC) for bone substitution. *Materials Science & Engineering C: Materials for Biological Applications*, 31, 740–747.

SUPPORTING INFORMATION

Additional supporting information may be found online in the Supporting Information section at the end of this article.

How to cite this article: Ramirez Caballero SS, Ferri-Angulo D, Debret R, et al. Combination of biocompatible hydrogel precursors to apatitic calcium phosphate cements (CPCs): Influence of the in situ hydrogel reticulation on the CPC properties. *J Biomed Mater Res*. 2020;1–15. <https://doi.org/10.1002/jbm.b.34685>